International Journal of Engineering Trends and Technology
ISSN: 2231 – 5381 / https://doi.org/10.14445/22315381/IJETT-V70I5P201
Volume 70 Issue 5, 1-8, May 2022

Original Article

Optical and Electrochromic Properties of CeO_2/WO_3 Hybrid Thin Films Prepared by Hydrothermal and Sputtering

Ashok Reddy G V [1], K Naveen Kumar [2], Habibuddin Shaik [3], R Imran Jafri [4], Ramachandra Naik [5], Doreswamy B H [6]

[1]*Department of Physics, Nitte Meenakshi Institute of Technology, Yelahanka, Bengaluru, Karnataka, India.*
[1]*Department of Physics, SJB Institute of Technology, Kengeri, Bengaluru, Karnataka, India.*
[2]*Department of Physics, and Center for Nanomaterials and MEMS, Nitte Meenakshi Institute of Technology, Yelahanka, Bengaluru, Karnataka, India.*
[3]*Department of Physics, and Center for Nanomaterials and MEMS, Nitte Meenakshi Institute of Technology, Yelahanka, Bengaluru, India.*
[4]*Department of Physics and Electronics, Christ University, Hosur Road, Bengaluru Karnataka, India.*
[5]*Department of Physics, New Horizon College of Engineering, Bengaluru, Karnataka, India.*
[6]*Department of Physics, SJB Institute of Technology, Kengeri, Bengaluru, Karnataka, India.*

ashokreddy.gv@nmit.ac.in

Received: 19 February 2022 Revised: 31 March 2022 Accepted: 22 April 2022 Published: 19 May 2022

Abstract *- Innovative chromogenic nanostructures like hybrids but also composite materials can be increased electrochromic efficiency because of their prospective application values in low-power displays, smart windows, electronic papers, and car anti-reflect mirrors. We used a hydrothermal approach to make Cerium oxide Nanorods have various ratios in this report. DC magnetron sputtering procedures cover the generated cerium oxide nanorods of various diameters with a tungsten oxide layer in one step. the surface plasmon effect varies depending on the size of Ce Nanorods, and this phenomenon impacts electrochromic results. the electrochromic performances of CeO_2/WO_3 nanorods on FTO-coated glass slides are examined using a 0.5 M solution of H_2SO_4 as the electrolyte in the visible range. These structures produce considerable optical modulation (47 %, 45 %, and 41 % at 700 nm) and coloration efficiency (11.6, 7.57, and 10.84 cm^2C^{-1} at 700 nm).*

Keywords *- Smart window, Nanocomposite, Cerium oxide nanorods, Thin film, Electrochromic.*

1. Introduction

Study in the electrochromic (EC) phenomena has risen in the latest years of increased global awareness of global warming, which has the potential to cut energy usage [1]–[4]. Electrochromic devices (ECDs) can be used in a variety of applications and green technologies, including power smart windows, because they are based on the permanent and reversible change of optical properties when an electric field is applied through them [5]–[9]. People would spend more than 80% of their daily lives in buildings and cars, so using smart windows in them was essential [3], [10][11]. in coloured mode, such devices absorbed more visible wavelengths, lowering optical transmittance and energy usage and lowering indoor thermal comfort during the summertime or peak hours. in opposite, in a bleached state, these devices reduce the quantity of absorption, resulting in high optical transmittance. Negative potentials (such as WO_3) are used to colour cathodic EC substances, while positive potentials (such as WO_3) are used to colour anodic EC materials (such as NiO). Metal oxide nanoparticles, including nickel, tungsten, manganese, cobalt, palladium, rhodium, molybdenum, iridium, titanium, ruthenium, and cerium oxides, are the most well-known inorganic EC materials [12]–[20]. Tungsten oxide is a particularly successful inorganic EC element that is commonly utilized in sunscreens (WO_3) [21]–[30]. in the following electrochemical procedure[31], [32], WO_3 coatings that have been coloured (dark blue for W6+ in WO_3) can be cleaned (clear W5+ in WO_3):

$$WO_3 + xe^- + xM+ \leftrightarrow MxWO_3 \ (M = H+, Li+, Na+)$$

Such changes in optical behaviour are caused by the injection and exertion of ions from liquid electrolyte adjacent to the EC surface that enters the microstructure of the hosting EC material networks. According to a recent study, WO3 inclusion with doping components greatly impacts device performance. For example, Bathe et al. have made a Ruthenium (Ru) doped WO3 thin film that outperforms pure WO3 thin film in cyclic stability by two times. the fabrication of crystalline WO3 nanorod arrays coated with molybdenum Mo.

Improve the colouring efficiency (η) of a sputtered amorphous WO_3 (30 % enhancement at the highest eye-sensitive wavelength of 520 nm for 0.57 wt % doping) [9]. However, there have been a few studies on the effects of Cerium oxide (a rare metals element) doped on the EC characteristics of WO_3.

Based on the structure of nanorod films with various aspect ratios, we employed a hydrothermal technique to create cerium oxide nanorods on top of DC magnetron sputtered tungsten oxide thin film was coated. the effect of coloured and bleached states on the EC characteristics of CeO_2/WO_3 nanorod-shell hybrid composites was explored using visible light spectroscopy and voltammetry (CV). This study aims to look into the electrochromic effect of Cerium oxide NRs cores as a rare earth metal and how this property may be used to improve EC performance in nanocomposite smart windows.

2. The Experiment's Specifics Include

2.1. Cerium Oxide Nanoparticles were Synthesized and Grown on FTO Substrates Actively

CeO_2 Nanorods were synthesized on a substrate of FTO-covered glasses. the substrates were cleaned to research specifications. the equipment used included an ultrasonicator, soap solution, acetone, and deionized water, and the substrates were nitrogen dried after the cleaning process. in one beaker, 1M urea (CO $(NH_2)_2$, Sigma Aldrich) was made, while in another, 0.1 M cerium nitrate hex hydrate ($Ce(NO_3)_36H_2O$, Sigma Aldrich) was made in deionized water. As illustrated in the equation below, combine the two solutions of 0.1M cerium nitrate hex hydrate and 1M urea:

$$CeO\ (NO_3)_36H2O+NH_2CONH_2 \leftrightarrow CeO2+N_2+CO_2+H_2O$$

To optimize the CeO_2 nanorods' shape, 10µL HCl was introduced to the reaction precursor for only a few samples. After another 20 minutes of stirring, the mixture was autoclaved in an 80 mL Teflon container. Figure 1 shows the FTO coating glasses upright against the Teflon container's wall, with the substrates properly positioned so that the FTO-coated side faces the Teflon container's wall. the autoclave was kept in a 100°C oven for 12 hours. After the synthesis was finished, the substrate was carefully cleaned with distilled water before being dried with nitrogen gas. Next, after 3-hour heat treatment in an air atmosphere dried at room temperature in a vacuum environment, crystalline cerium oxides NRs were produced. the cerium oxide NRs bonded well to the FTO substrates.

Fig. 1 Hydrothermal process autoclave

2.2. CeO_2 nanorods are used to coat WO_3 thin films

The sputtering process was employed with a 3-inch diameter Tungsten (W) target in an argon and oxygen atmosphere**.** Cerium oxide nanorods grown on FTO were used as substrates to deposit WO3 films. the substrates were kept 9 cm from the target throughout the deposition. the temperature of the substrates was kept at 300 K. the highest vacuum of the sputtering equipment used in this investigation is 1×10^{-6} mbar. the vacuum chamber was connected with a 1000 LPS TM pump and a 1000 LPM rotary vane pump. the target was pre-sputtering in an argon atmosphere for 15 minutes before each deposition to assure that it was impurity-free. At various oxygen partial pressures (ppO2), including $8x10^{-4}$ ppO2, WO3 films were created. Pure WO_3 film, as deposited CeO_2/WO_3 film, annealed CeO_2/WO_3 film, and 10 µL HCL CeO_2/WO_3 film were termed 1, 2, 3, and 4 correspondingly for samples made by both hydrothermal and sputtered techniques as shown table1.

3. Characterization

SEM was used to investigate the surface characterization of nanocomposite films. Scanning Electron Microscopy (SEM) is a type of microscopy that examines objects using electrons (SEM, Being Nano-Instruments TESCAN-VEGA3 LMU Instruments, resolution 3.0nm at 30Kv, maximum field of view 0.08m, tungsten heated cathode electron gun, tungsten heated cathode electron gun). the results of element identification are acquired via energy-dispersive X-ray spectroscopy (EDX). X-ray Diffraction (XRD, range: -400 to +2200, step size: 0.0010) With the components inserted, the reproducibility is +0.00010. the crystalline structure of the film was examined using Resolution: 0.0290 2 and PLXcel@21.40 (low angle) 2. A SPECORD ultraviolet-visible spectrometer was used to test the optical absorption performance, with FTO glass (Optical band gap: >4 eV) functioning as a blank. All electrochemical experiments were carried out using an SP 300 electrochemical workstation. A three-electrode electrochemical cell examined the electrochromism of WO3, CeO2/WO3 sheets. A CeO_2/WO_3 film was coated on an FTO substrate (1.5 cm x 1.5 cm), a platinum wire counter electrode, and a $Hg/HgCl_2$ reference electrode (1 M KCl). the applied sweep voltage was maintained from -0.7 V to +1 V with 0.1 V/s step size in an aqueous solution of 0.5 M H_2SO_4 electrolyte for all cyclic-voltammetry (C-V) tests at scan speeds of 10 mV/s. All-optical transmittance tests were carried out using applied potential (from -0.7 to +1.0 V) to study the bleached and coloured states.

4. Discussion of the Results

4.1. Morphological Studies

According to SEM pictures, CeO_2 nanorods formed successfully on fluorine-doped tin oxide (FTO) substrates. CeO_2 nanorods with different morphologies were synthesized on the substrate using the same growth solution concentrations and conditions (Fig. 2). As deposited cerium oxide nanorods, annealed cerium oxide nanorods, and 10 µL HCL were the grown CeO_2 nanorods

roughly became longer and thinner with diameters of about 857± 152 nm, 560 ± 32 nm, and 423 ± 24 nm and lengths of about 1.013± 44 µm, 1.369± 65 µm, and 1.66 ± 78 µm respectively, due to in greater density of CeO_2 nanorods. the cerium oxide NRs formed flower-like morphologies of numerous nanorods with tiny diameters in a 10 µL HCL solution of cerium nitrate hexahydrate (Fig. 2 c, right). Fewer crystal nuclei were produced when HCl was not given to the solution of cerium nitrate hex hydrate and urea, which encouraged future growth. As a result, a larger diameter nanocluster was eventually produced. When a sufficient quantity of HCl (10 µL) was added to the cerium nitrate hex hydrate and urea solution, many small CeO_2 nanorods were produced fast, resulting in slow further growth. Due to the enormous active, effective surface area of the produced tiny nanorods, a well-aligned CeO_2 nanorods array was obtained. To form the branched CeO_2 nanorods array, the optimal amount of HCl should be found in a small range. Under varying HCl concentrations, the development process of WO_3 nano three, nanowire, and nanocluster arrays on FTO glass yielded similar results [33].

The as-sputtered pure WO_3 sheet's SEM surface morphologies reveal a nonporous morphology (Fig. 2 d) and highlight its amorphous surface structure by showing a homogeneous, smooth, and crack-free surface. the film's surface morphology is affected by the CeO_2 deposited, annealed, and additions of 10 µL HCL. Surface roughness rose as the number of CeO_2 nanorods grew. on the surfaces of CeO_2/WO_3 films, nanorods connected to cerium oxide may be easily seen (Fig. 2 e).

4.2. EDS Analysis

Figure 3 shows the compositions and elemental observations of pure cerium oxide Nanorods, pure WO_3, and WO_3 thin films coated on cerium oxide Nanorods using EDS spectra. the energy region of the EDS spectrum was 0 to 15.3 KeV. There are conventional peaks of Ce and O atoms (figure 3a), O and W (figure 3b), and Ce, W, and O atoms (figure 3c) in the provided spectra, but no further recognizable peaks are visible [34]. This indicates that no additional impurities form in the cerium oxide Nanorods, WO_3 film, and CeO_2/WO_3 film. the quality of CeO_2 Nanorods produced by the hydrothermal approach and CeO_2/WO_3 thin films deposited by DC Magnetron Sputtering was excellent. Hydrothermal methods CeO_2 Nanorods on sputtered tungsten oxide films, pure WO_3 film by DC magnetron sputtered, and hydrothermal methods CeO_2 Nanorods on sputtered tungsten oxide films did not completely satisfy the stoichiometric ratios of cerium and oxygen, tungsten and oxygen, and cerium, tungsten, and oxygen respectively as shown in the table2.

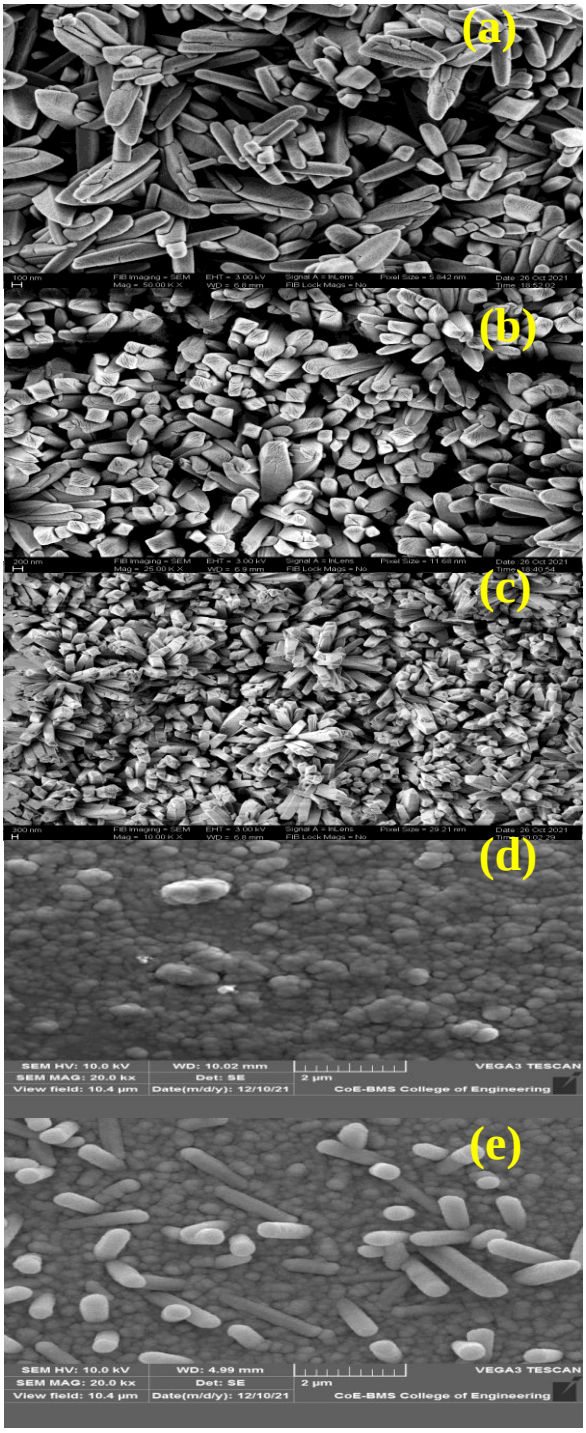

Fig. 2 SEM images of CeO_2 Nanorods by hydrothermal processes (a) as-deposited (b) annealed at 350^{0}C at 3hours (c) 10 µL HCL annealed at 350^{0}C at 3 hours (d) pure WO_3 by sputtered method and (e) WO_3 on CeO_2 Nanorods

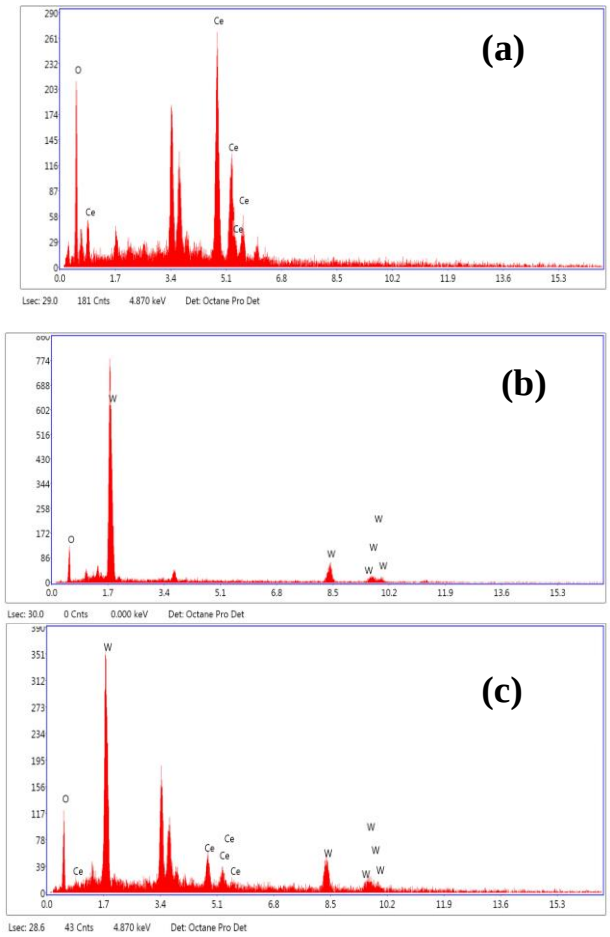

Fig. 3 EDX images of (a) pure CeO_2 Nanorods by hydrothermal method (b) pure wo3 film by sputtered method (c) CeO_2/WO_3 hybrid film.

Table 1. Shows the parameters used to grow CeO_2 Nanorods

Sample name	Sample number	Auto cleave temperature (^{0}C)	Annealed temperature(^{0}C)	Sputtered time for tungsten oxide (minutes)
Pure WO_3	1	100	----------	18
10µl HCL CeO_2/WO_3	2	100	350	18
Annealed CeO_2/WO_3	3	100	350	18
As deposited CeO_2/WO_3	4	100	--------	18

4.3. XRD analysis

The XRD patterns of pure WO_3 by sputtered, CeO_2 nanorods generated by hydrothermal technique, and CeO_2/WO_3 Nanoporous structure for the sample are shown in Figure 4**.** Only diffraction patterns from the FTO substrate are visible in the XRD pattern of the pure WO_3 film sputtered at room temperature, whereas WO_3's characteristic diffraction peaks are absent, indicating the films' amorphous phase. the existence of peaks indicates that the nanorods are crystalline. Thermal treatment of the as-grown NRs resulted in CeO_2 NRs with patterns similar to face-centred cubic CeO2 with a lattice constant of a=5.4104 nm [35]. (See Figure 4), Peaks can be seen at 2Θ=26.68^0, 33.90^0, 54.81^0, 61.59^0, and 65.53^0 in reflections from the (111), (200), (311), (222), and (400) planes, which correspond to the face-centred cubic phase of CeO_2 [36]. the most noticeable effect of annealing CeO2 nanorods on any film process is a change in film crystallinity, which may be examined using XRD. As a result, XRD analysis was used to characterize the CeO_2/WO_3 films to explore the crystal structure modification. Peaks observed at 2Θ = 26.80º, 28.88º, 34.12º, 38.06^0, and 51.85º, which are reflections from the (222), (023), (-204), (-242), and (-126) are WO_3 films deposited onto crystalline CeO_2 nanorods of nanocomposites. This crystalline CeO_2/WO_3 has electrochromic components and the ability to recombination photo-generated holes and electrons during the process [37].

Table 2. the EDX analysis of pure CeO_2 Nanorods, pure WO_3, and CeO_2/WO_3 films

Figure name	Element	Weight %	Atomic %
a	Oxygen	26.85	76.27
	Cerium	73.15	23.73
b	Oxygen	34.28	85.70
	Tungsten	65.72	14.30
c	Oxygen	28.63	80.92
	Cerium	19.81	6.39
	Tungsten	51.56	12.68

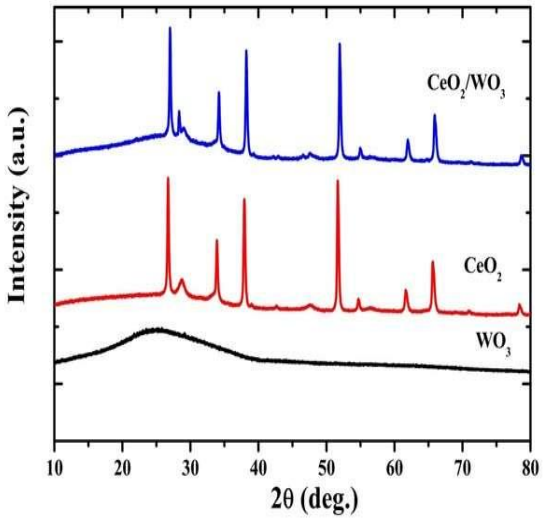

Fig. 4 XRD patterns of pure WO_3, CeO_2 nan rods and CeO_2/WO_3 Nanocomposite sample

4.4. Optical Characteristics

In fig.5a, transmittance plots of wo_3 thin films over cerium oxide Nanorods were exhibited for pure WO_3 film, as deposited CeO_2/WO_3 film, annealed CeO_2/WO_3 film, and 10 µL HCL CeO_2/WO_3 films. At ambient temperature, all of the samples were deposited. It was reported that annealing and adding 10 µL HCL to CeO2/WO3 thin films enhanced their transmittance and that the optical properties of CeO2 Nanorods are dependent on how they are formed, annealed, and treated. At a wavelength of 700 nm, the 10 µL HCL CeO_2/WO_3 film has a greater transmittance of more than 40%. At a wavelength of 700nm, the deposited CeO_2/WO_3 film has a transmittance of 25%, while the annealed CeO_2/WO_3 film has a transmittance of 40%. the increased scattered light losses were ascribed to the increased surface roughness of the CeO_2/WO_3 films as deposited.

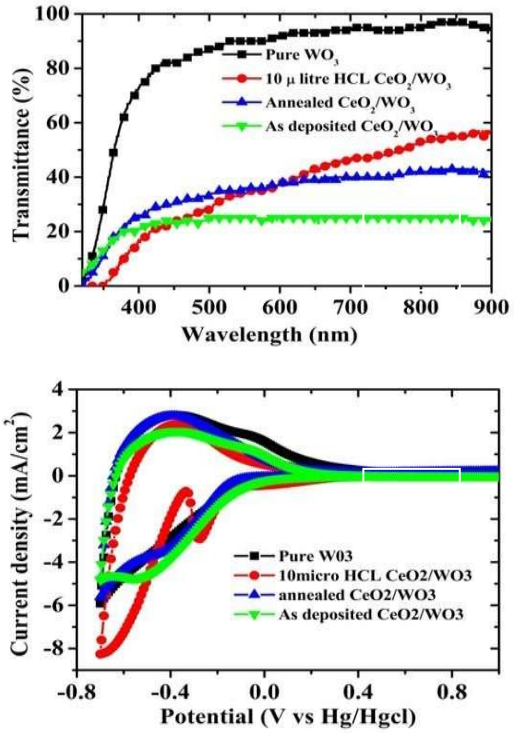

4.5. Properties of Electrochromic Materials

The electrochemical performance of the electrochromic CeO_2/WO_3 impacts its design. the half-cell CV curves of cerium oxide Nanorods on tungsten oxide (CeO_2/WO_3) films were recorded in 0.5 M H_2SO_4 solution at a scan rate of 10 mVs^{-1} in the applied potential of -0.7 V to 1 V. Figure 6 b indicates the CV curves of cerium oxide Nanoparticles on deposited WO_3 film. H+ ion insertion and extraction into CeO2/WO3 films are indicated by the CV characteristics in Fig. 5 b, which show typical wider featureless peaks. the cathodic peak current also works as a measurement for the rate of H^+ ion insertion, with a lower current suggesting a faster reaction rate. the CV curves' cathodic peak current (recorded at -0.7V) originally increased from -8.25 mA at sample no 4 to -4.81 mA at sample no 2, the smallest cathodic peak current of all CV curves. Table 3 shows that pure WO_3 in a sputtered film increases the cathodic peak current to -5.92 mA. H^+ ions and electrons diffuse more easily into annealed and 10 µL HCL CeO2/WO3 films than they used to into deposited CeO_2/WO_3 films, resulting in lower cathodic peak current.

Table 3. Diffusion coefficients for pure WO_3 and CeO_2/WO_3 films

Sample name	Cathodic peak current i_{cp} (mA)	D_{CP} (cm^2/s)
1	-5.92	3.86×10^{-14}
2	-4.81	2.54×10^{-14}
3	-5.62	3.48×10^{-14}
4	-8.25	7.5×10^{-14}

Table 4. Optical modulation and Coloration efficiency for pure WO_3 and CeO_2/WO_3 films

Sample name	Bleached T_b (%)	Coloured T_c (%)	Optical modulation $\Delta OD=T_b-T_c$	CE (cm^2/s)
1	48	6	42	7.60
2	54	9	45	7.57
3	45	4	41	10.84
4	49	2	47	11.60

At 10 HCL cerium oxide nanorods, the charge for CeO_2/WO_3 films changes dramatically. As the cerium oxide content was deposited, annealed, and 10 HCL, variations in electrochromic properties and optical transmittance of CeO_2/WO_3 hybrid films were detected. the change of cathodic peak current and diffusion co-efficiency of samples 1 to 4 is shown in Figure 7 c. the reduction/oxidation peak currents [(i_{pa}) and (i_{pc})] colouring efficiency and diffusion coefficient have all been examined using cyclic voltammograms, as shown in Randles Sevcik equation [38].

$$ip = n^{3/2} x\, D^{1/2} x\, C_0 \,x\, A\, x 2.69 \times 10^5 \times v^{1/2} \qquad (1)$$

The number of electrons is represented by n, the ions diffusion coefficient is represented by D, the peak current is represented by ip, the active CeO_2/WO_3 film area is represented by A, and the scan rate is represented by v, and Co represents the electrolyte concentration.

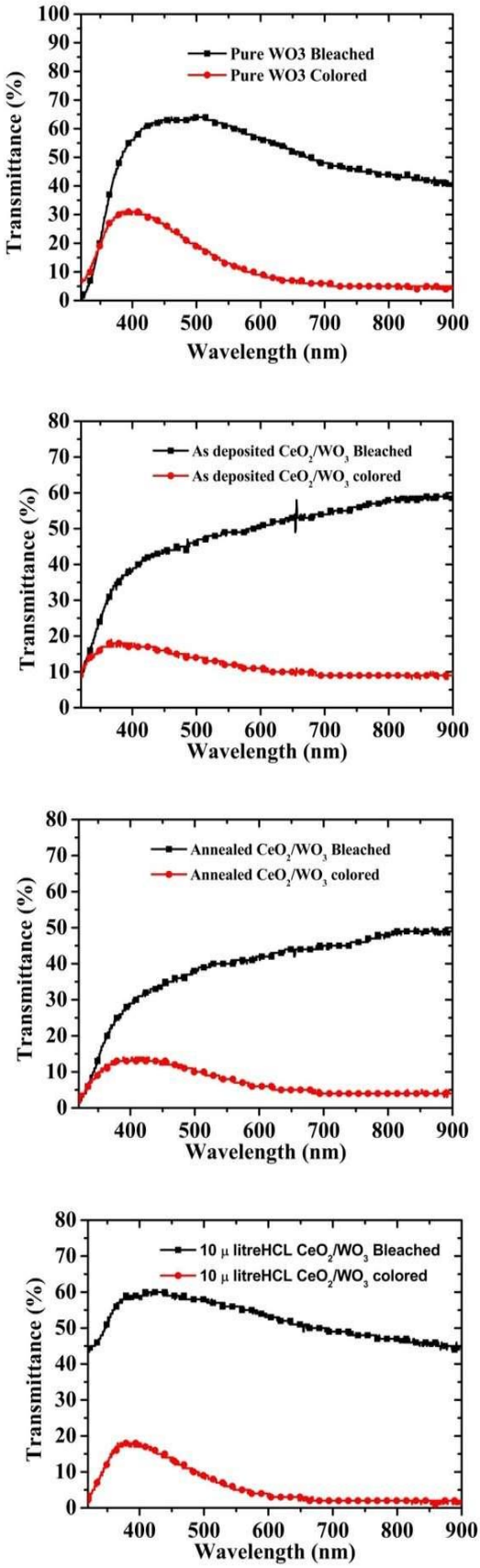

Fig. 6 Bleached and coloured transmittances of CeO_2/WO_3 films for a) Pure WO_3, b) As deposited CeO_2/WO_3film c) Annealed CeO_2/WO_3 film and d) 10µL CeO_2/WO_3 film

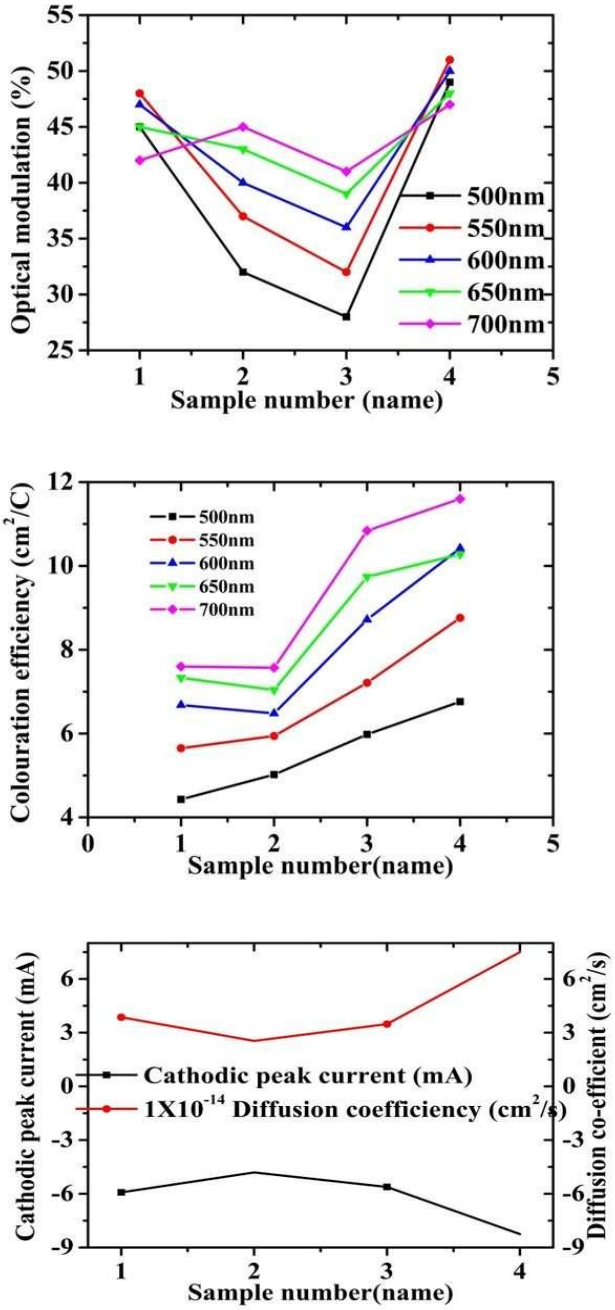

Fig 7 (a) Optical modulation (b) colouration efficiency at a wavelength from 500nm to 700nm with various samples of cerium oxide (c) Cathodic peak current and diffusion co-efficiency with various samples of cerium oxide on wo_3 films

Optical transmittance changes due to ion chemical interaction (coloured state) and deintercalation (bleached state) have been recorded during the CV. Figures 6a-d demonstrate the optical transmittance of coloured and bleached Cerium oxide Nanoparticles on coated WO_3 films for various CeO_2/WO_3 film samples ranging from 1 to 4. CeO_2/WO_3 films were coloured at the cathode potential (-0.7V) because some ions were reduced from W^{6+} ions to W^{5+} ions owing to ion deintercalation, while CeO_2/WO_3 films were bleached at the anodic potential (1V) because few ions increased from W^{5+} ions to $W6^{+}$ ions due to ion deintercalation. According to cerium oxide nanorods annealed and 10µL HCL, the charges of de-intercalated

and intercalated H^+ ions in the CeO_2/WO_3 film change. the transparency spectra for CeO_2/WO_3 films produced by sputtering for various samples of cerium oxide nanorods are presented in Fig. 6a-d. the transmittance of coloured and bleached states changes as the cerium oxide is annealed and 10 µL HCL. At 700nm, the bleached state transmittance of 10 µL HCL CeO_2/WO_3 film deposition annealed samples was 49%, while the coloured state transmittance was 2%. in cerium oxide nanorods that have not been annealed, the transmittance of coloured and bleached states exhibits a decrease.

Use the formula below to determine colouring efficiency:

$$\eta \text{ or } CE = \Delta OD / (Qi/A) \quad (2)$$

Where CE stands for colourations efficiency, a charge of in electrode was Q, ΔOD stands for optical density, and A stands for the area of the CeO_2/WO_3 sheet that had to operate as an electrode. Use the equation below to determine ΔOD (3).

$$\Delta OD = \log - (T_b/ T_c) \quad (3)$$

T_b and T_c are the transparency of the bleached and coloured states, respectively. At wavelengths of 500nm–700nm, colouration efficiency values were computed using pure WO_3, as-deposited, annealed, and 10 µL HCL cerium oxide concentration. With wavelengths varying from 500nm to 700nm, the colouring efficiency and optical modulation of cerium oxide hybrid films shown in Fig. 7a-b were modified. Coloration efficiency calculated for CeO_2/WO_3 films at a wavelength of 650 nm was 7.33 cm^2 C^{-1}, 7.04 cm^2 C^{-1}, 9.74 cm^2 C^{-1}, and 10.28 cm^2 C^{-1} for cerium oxide concentrations of samples 1,2,3 and 4, and 700 nm was 7.60 cm^2 C^{-1}, 7.57 cm^2 C^{-1}, 10.84 cm^2 C^{-1}, and 11.6 cm^2 C^{-1} respectively. the difference in colouring efficiency and optical modulation of cerium oxide in different samples was shown in Figures 7a-b. the CE of the 10 µL HCL CeO_2/WO_3 film was the highest because the surface-to-volume ratios and porous CeO_2/WO_3 thin films were high compared to other pure WO_3 and CeO_2/WO_3 thin films. As a result, more H^+ ions successfully occur in the presence of the CeO_2/WO_3 film.

5. Conclusion

As an aspect of the hydrothermal process, CeO_2 nanorods of various sizes are as-deposited, annealed, and 10 µL HCL. the CeO_2 nanorods were synthesized and coated with tungsten oxide shells, and CeO_2/WO_3 nanocomposite films were effectively deposited on FTO-coated glass substrates using the DC magnetron sputtered coating process. the structural study of nanocomposites reveals that the products contained cerium oxide and tungsten oxide in non-stoichiometric percentages. Moreover, cyclic voltammetry correlated to various sizes and shapes of cerium oxide nanorods in nanocomposite hybrid films improves EC hybrid films compared to pure WO_3 thin film. Samples have a significant optical modulation (41 %, 45 %, and 47 % at 700 nm) as well as a considerable colouring efficiency (7.57, 10.84, and 11.6 cm^2/ C^{-1} at 700 nm). This study found that this structure can be implemented in smart windows that have a significant CE and satisfactory optical modulation

Acknowledgment

Our sincere thanks to AICTE, New Delhi, India, for granting our research. Ref: 8-39/RIFD/RPS/POLICY-1/2016-2017.

References

[1] M. Kamalisarvestani, R. Saidur, S. Mekhilef, and F. S. Javadi, Performance, Materials and Coating Technologies of Thermochromic Thin Films on Smart Windows, Renew. Sustain. Energy Rev., 26 (2013) 353–364. Doi: 10.1016/J.Rser.2013.05.038.

[2] J. Xu, S. Shi, X. Zhang, Y. Wang, M. Zhu, and L. Li, Structural and Optical Properties of (Al, K)-Co-Doped Zno Thin Films Deposited By A Sol-Gel Technique, Mater. Sci. Semicond. Process., 16(3) (2013) 732–737. Doi: 10.1016/J.Mssp.2012.12.016.

[3] C. F. Azevedo Et Al., New Thin Films of Nio Doped With V2o5 For Electrochromic Applications, J. Phys. Chem. Solids, 110 (2017) 30–35. Doi: 10.1016/J.Jpcs.2017.05.021.

[4] J. Gutpa, H. Shaik, K. Naveen Kumar, and S. A. Sattar, Pvd Techniques Proffering Avenues for Fabrication of Porous Tungsten Oxide (Wo3) Thin Films: A Review, Mater. Sci. Semicond. Process., 143 (2022) 106534. Doi: 10.1016/J.Mssp.2022.106534.

[5] S. Adhikari Et Al., Electrochemical Protonation/De-Protonation of Titania Nanotubes Decorated with Silver Phosphate Crystals: an Enhanced Electrochromic Color Contrast, Opt. Mater. (Amst)., 40 (2015) 112–117. Doi: 10.1016/J.Optmat.2014.12.004.

[6] D. Chatzikyriakou, A. Maho, R. Cloots, and C. Henrist, Ultrasonic Spray Pyrolysis As A Processing Route For Templated Electrochromic Tungsten Oxide Films, Microporous Mesoporous Mater., 240 (2017) 31–38. Doi: 10.1016/J.Micromeso.2016.11.001.

[7] K. Sauvet, L. Sauques, and A. Rougier, Electrochromic Properties of Wo3 As A Single Layer and in A Full Device: From the Visible To the Infrared, J. Phys. Chem. Solids, 71(4) (2010) 696–699. Doi: 10.1016/J.Jpcs.2009.12.069.

[8] E. Eren, C. Alver, G. Yurdabak Karaca, E. Uygun, and A. Uygun Oksuz, Enhanced Electrochromic Performance of Wo3 Hybrids using Polymer Plasma Hybridization Process, Synth. Met., 235(2017) (2018) 115–124. Doi: 10.1016/J.Synthmet.2017.12.003.

[9] Y. Yin, C. Lan, S. Hu, and C. Li, Effect of Gd-Doping on Electrochromic Properties of Sputter Deposited Wo3 Films, J. Alloys Compd., 739 (2018) 623–631. Doi: 10.1016/J.Jallcom.2017.12.290.

[10] K. J. Patel, G. G. Bhatt, J. R. Ray, P. Suryavanshi, and C. J. Panchal, All-Inorganic Solid-State Electrochromic Devices: A Review, J. Solid State Electrochem., 21(2) (2017) 337–347. Doi: 10.1007/S10008-016-3408-Z.

[11] C. J. Tang, J. M. Ye, Y. T. Yang, and J. L. He, Large-Area Flexible Monolithic Ito/Wo3/Nb2o5/Nivoχ/Ito Electrochromic Devices Prepared By using Magnetron Sputter Deposition, Opt. Mater. (Amst)., 55 (2016) 83–89. Doi: 10.1016/J.Optmat.2016.03.021.

[12] I. Kostis Et Al., Highly Porous Tungsten Oxides For Electrochromic Applications, Microelectron. Eng., 111 (2013) 149–153. Doi: 10.1016/J.Mee.2013.03.039.
[13] C. R. Dhas, R. Venkatesh, R. Sivakumar, A. M. E. Raj, and C. Sanjeeviraja, Effect of Solution Molarity on Optical Dispersion Energy Parameters and Electrochromic Performance of Co3o4 Films, Opt. Mater. (Amst)., 72 (2017) 717–729. Doi: 10.1016/J.Optmat.2017.07.026.
[14] D. Dong Et Al., Electrochromic Properties of Nio X :H Films Deposited By Dc Magnetron Sputtering For Ito/Nio X :H/Zro 2 /Wo 3 /Ito Device, Appl. Surf. Sci., 357 (2015) 799–805. Doi: 10.1016/J.Apsusc.2015.09.056.
[15] S. Leinberg Et Al., Switchable Optical Transmittance of Tio2 Submicron-Diameter Wire Suspension-Based Smart Window Device, Opt. Mater. (Amst)., 46 (2015) 418–422. Doi: 10.1016/J.Optmat.2015.04.057.
[16] T. N. Lin, Y. H. Lin, C. T. Lee, S. Han, and K. W. Weng, Electrochromic Properties of Bipolar Pulsed Magnetron Sputter Deposited Tungsten-Molybdenum Oxide Films, Thin Solid Films, 584 (2015) 341–347. Doi: 10.1016/J.Tsf.2014.12.036.
[17] S. Ulrich, C. Szyszko, S. Jung, and M. Vergöhl, Electrochromic Properties of Mixed Oxides Based on Titanium and Niobium For Smart Window Applications, Surf. Coatings Technol., 314 (2017) 41–44. Doi: 10.1016/J.Surfcoat.2016.11.078.
[18] S. Stojkovikj, M. Najdoski, V. Koleva, and S. Demiri, Preparation of Electrochromic Thin Films By Transformation of Manganese(Ii) Carbonate, J. Phys. Chem. Solids, 74(10) (2013) 1433–1438. Doi: 10.1016/J.Jpcs.2013.05.001.
[19] Z. Chen, A. Xiao, Y. Chen, C. Zuo, S. Zhou, and L. Li, Highly Porous Nickel Oxide Thin Films Prepared By A Hydrothermal Synthesis Method For Electrochromic Application, J. Phys. Chem. Solids, 74(11) (2013) 1522–1526. Doi: 10.1016/J.Jpcs.2013.05.015.
[20] J. Gupta, H. Shaik, and K. N. Kumar, A Review on the Prominence of Porosity in Tungsten Oxide Thin Films For Electrochromism, Ionics (Kiel)., 27(6) (2021) 2307–2334. Doi: 10.1007/S11581-021-04035-8.
[21] V. R. Buch, A. K. Chawla, and S. K. Rawal, Review on Electrochromic Property for Wo3 Thin Films using Different Deposition Techniques, Mater. Today Proc., 3(6) (2016) 1429–1437. Doi: 10.1016/J.Matpr.2016.04.025.
[22] C. Dulgerbaki, A. I. Komur, N. Nohut Maslakci, F. Kuralay, and A. Uygun Oksuz, Synergistic Tungsten Oxide/Organic Framework Hybrid Nanofibers For Electrochromic Device Application, Opt. Mater. (Amst)., 70 (2017) 171–179. Doi: 10.1016/J.Optmat.2017.05.024.
[23] G. Leftheriotis, E. Koubli, and P. Yianoulis, Combined Electrochromic-Transparent Conducting Coatings Consisting of Noble Metal, Dielectric and Wo3 Multilayers, Sol. Energy Mater. Sol. Cells, 116 (2013) 110–119. Doi: 10.1016/J.Solmat.2013.04.013.
[24] H. Li Et Al., Constructing Three-Dimensional Quasi-Vertical Nanosheet Architectures from Self-Assemble Two-Dimensional Wo 3 ·2h 2 O For Efficient Electrochromic Devices, Appl. Surf. Sci., 380 (2016) 281–287. Doi: 10.1016/J.Apsusc.2016.01.009.
[25] H. Najafi-Ashtiani and A. Bahari, Optical, Structural and Electrochromic Behavior Studies on Nanocomposite Thin Film of Aniline, O-Toluidine and Wo3, Opt. Mater. (Amst)., 58 (2016) 210–218. Doi: 10.1016/J.Optmat.2016.05.035.
[26] Y. Yue Et Al., High-Performance Complementary Electrochromic Device Based on Wo3·0.33h2o/Pedot and Prussian Blue Electrodes, J. Phys. Chem. Solids, 110 (2017) 284–289. Doi: 10.1016/J.Jpcs.2017.06.022.
[27] R. Mukherjee and P. P. Sahay, Improved Electrochromic Performance in Sprayed Wo3 Thin Films Upon Sb Doping, J. Alloys Compd., 660 (2016) 336–341. Doi: 10.1016/J.Jallcom.2015.11.138.
[28] K. N. Kumar Et Al., Sputter Deposited Tungsten Oxide Thin Films and Nanopillars : Electrochromic Perspective, Mater. Chem. Phys., 278(2021) (2022) 125706. Doi: 10.1016/J.Matchemphys.2022.125706.
[29] K. Naveen Kumar Et Al., on Ion Transport During the Electrochemical Reaction on Plane and Glad Deposited Wo3 Thin Films, Mater. Today Proc., (2021) Doi: 10.1016/J.Matpr.2021.11.113.
[30] K. Naveen Kumar, H. Shaik, Sathish, V. Madhavi, and S. Abdul Sattar, on the Bonding and Electrochemical Performance of Sputter Deposited Wo3 Thin Films, Iop Conf. Ser. Mater. Sci. Eng., 872(1) (2020). Doi: 10.1088/1757-899x/872/1/012147.
[31] E. Koubli, S. Tsakanikas, G. Leftheriotis, G. Syrrokostas, and P. Yianoulis, Optical Properties and Stability of Near-Optimum Wo3/Ag/Wo3 Multilayersfor Electrochromic Applications, Solid State Ionics, 272 (2015) 30–38. Doi: 10.1016/J.Ssi.2014.12.015.
[32] E. Ahmadi, C. Y. Ng, K. A. Razak, and Z. Lockman, Preparation of Anodic Nanoporous Wo3film using Oxalic Acid As an Electrolyte, Elsevier Bv, 704 (2017).
[33] G. F. Cai, J. P. Tu, D. Zhou, X. L. Wang, and C. D. Gu, Growth of Vertically Aligned Hierarchical Wo3 Nano-Architecture Arrays on Transparent Conducting Substrates with Outstanding Electrochromic Performance, Sol. Energy Mater. Sol. Cells, 124 (2014) 103–110. Doi: 10.1016/J.Solmat.2014.01.042.
[34] R. Siva Prakash, C. Mahendran, J. Chandrasekaran, R. Marnadu, and S. Maruthamuthu, Impact of Substrate Temperature on the Properties of Rare-Earth Cerium Oxide Thin Films and Electrical Performance of P-Si/N-Ceo2 Junction Diode, J. Inorg. Organomet. Polym. Mater., 30(12)(2020) 5193–5208.Doi: 10.1007/S10904-020-01667-7.
[35] Z. Ji Et Al., Designed Synthesis of Ceo 2 Nanorods and Nanowires for Studying Toxicological Effects of High Aspect Ratio Nanomaterials, Acs Nano, 6(6) (2012) 5366–5380. Doi: 10.1021/Nn3012114.
[36] Y. J. Cho, H. Jang, K. S. Lee, and D. R. Kim, Direct Growth of Cerium Oxide Nanorods on Diverse Substrates for Superhydrophobicity and Corrosion Resistance, Appl. Surf. Sci., 340 (2015) 96–101. Doi: 10.1016/J.Apsusc.2015.02.138
[37] D. Channei, K. Chansaenpak, S. Phanichphant, P. Jannoey, W. Khanitchaidecha, and A. Nakaruk, Synthesis and Characterization of Wo3/Ceo2heterostructured Nanoparticles for Photodegradation of Indigo Carmine Dye, Acs Omega, 6(30) (2021) 19771–19777. Doi: 10.1021/Acsomega.1c02453.
[38] M. B. Babu and K. V. Madhuri, Synthesis and Electrochromic Properties of Nanocrystalline Wo3 Thin Films, Phys. B Condens. Matter, 584(2019) (2020) 412068. Doi: 10.1016/J.Physb.2020.412068.